Molecular Transport

International Edition: DOI: 10.1002/anie.201700166
German Edition: DOI: 10.1002/ange.201700166

Dynamic Gradient Directed Molecular Transport and Concentration in Hydrogel Films

*Tsung-Han Tsai, Mohammad A. Ali, Zhelong Jiang, and Paul V. Braun**

Abstract: *Materials which selectively transport molecules along defined paths offer new opportunities for concentrating, processing and sensing chemical and biological agents. Here, we present the use of traveling ionic waves to drive molecular transport and concentration of hydrophilic molecules entrained within a hydrogel. The traveling ionic wave is triggered by the spatially localized introduction of ions, which through a dissipative ion exchange process, converts quaternary ammonium groups in the hydrogel from hydrophilic to hydrophobic. Through a reaction–diffusion process, the hydrophobic region expands with a sharp transition at the leading edge; it is this sharp gradient in hydrophilicity that drives the transport of hydrophilic molecules dispersed within the film. The traveling wave moved up to 450 μm within 30 min, while the gradient length remained 20 μm over this time. As an example of the potential of molecular concentration using this approach, a 70-fold concentration of a hydrophilic dye was demonstrated.*

Methods for driving selective molecular transport through external forces are well established (e.g. gel electrophoresis, diffusiophoresis and chromatography),[1a] and approaches utilizing molecular motors[1b] or chemical potential gradients[2] to drive molecular transport are becoming widely discussed in the literature. Use of surfaces containing chemical gradients to drive the motion of biological cells,[2a] liquid droplets,[2b] nanoparticles,[2c] adamantine-appended dye molecules,[2d] poly(ethylene glycol),[2e] and poly(propyleneimine) dendrimers[2f] is now well established. Recently, we reported that charged molecules can be directionally transported, concentrated and separated within polyacrylamide hydrogel films containing built-in chemical potential gradients.[2g,h] However, in all these cases, the gradient was static, and thus the rate of chemical transport was sluggish since the slope of the chemical gradient was not steep (the gradient length was long).

As a way to create a propagating chemical gradient, we considered the use of reaction–diffusion (RD) chemistries. RD processes are common in nature, where they serve to govern the motion of molecules and information.[3] Synthetic RD systems[4] include chemical oscillations[5] based on the classic Belousov–Zhabotinsky (BZ) reaction,[6] which have been shown to yield far from equilibrium spatiotemporally evolving patterns. Other remarkable non-equilibrium patterns generated by RD processes are Turing structures.[7] Synthetic systems based on self-oscillating gels which convert chemical energy into mechanical energy[8] have been demonstrated to transport objects through the oscillatory swelling of a hydrogel based on the BZ reaction.[9] As far as we are aware, however, utilizing RD process to drive molecular transport is still unexplored.

We suggest a dynamic gradient (a "traveling wave") formed by a coupled RD process offers a powerful approach to overcome the slow kinetics of static chemical gradient assisted directional molecular transport and drive rapid molecular transport. The dynamic gradient investigated here is triggered by a RD process consisting of the spatially localized introduction of ions into the hydrogel which initially locally converts an analyte-containing hydrogel film from hydrophilic to hydrophobic. As the ions continue to enter and diffuse through the hydrogel, the ion-exchanged region expands, and hydrophilic molecules are pushed ahead of the expansion front (Figure 1).

A quaternary ammonium group-containing hydrogel is particularly useful for generating such a gradient, because the hydrophobicity of the quaternary ammonium group is highly counterion dependent. For example, it was shown that the water contact angle of a quaternary ammonium-containing polymer brush changed from 35° to 90° when counterion was changed from Cl^- to bis(trifluoromethane)sulfonamide ($TFSi^-$).[10] More broadly, the quaternary ammonium group hydrophobicity was found to increase with counterion in the order $Cl^- < Br^- < I^- < SCN^- < TFSi^-$ following a Hofmeister-type series.[11] Here, quaternary ammonium containing polyelectrolyte hydrogel films with various ammonium group chemistries and various counterions were investigated as the basis for the dynamic gradients (chemical details provided in Figure 1b).

To generate the dynamic gradient, 2 M bis(trifluoromethane)sulfonimide lithium (LiTFSi) aqueous salt solution was passed through a microchannel placed on top of the hydrogel film (Figure 1a, see the Supporting Information (SI) for the experimental setup). Upon exposure to LiTFSi, the quaternary ammonium group rapidly exchanged its counterion from Cl^-, I^-, or SCN^- to $TFSi^-$ because of the selective binding affinity of the quaternary ammonium group to $TFSi^-$ following a Hofmeister-type series,[11] making the hydrogel considerably more hydrophobic. LiTFSi continued to diffuse out of the microchannel, into and through the hydrogel driving

[*] Dr. T.-H. Tsai, Dr. M. A. Ali, Z. Jiang, Prof. P. V. Braun
Department of Materials Science and Engineering, Department of Chemistry, Beckman Institute for Advanced Science and Technology, Frederick Seitz Materials Research Laboratory, University of Illinois at Urbana Champaign
Urbana, IL 61801 (USA)
E-mail: pbraun@illinois.edu

Supporting information for this article (experimental procedure, additional results and characterizations of dynamic gradients, as well as numerical study and COMSOL simulation) can be found under http://dx.doi.org/10.1002/anie.201700166.

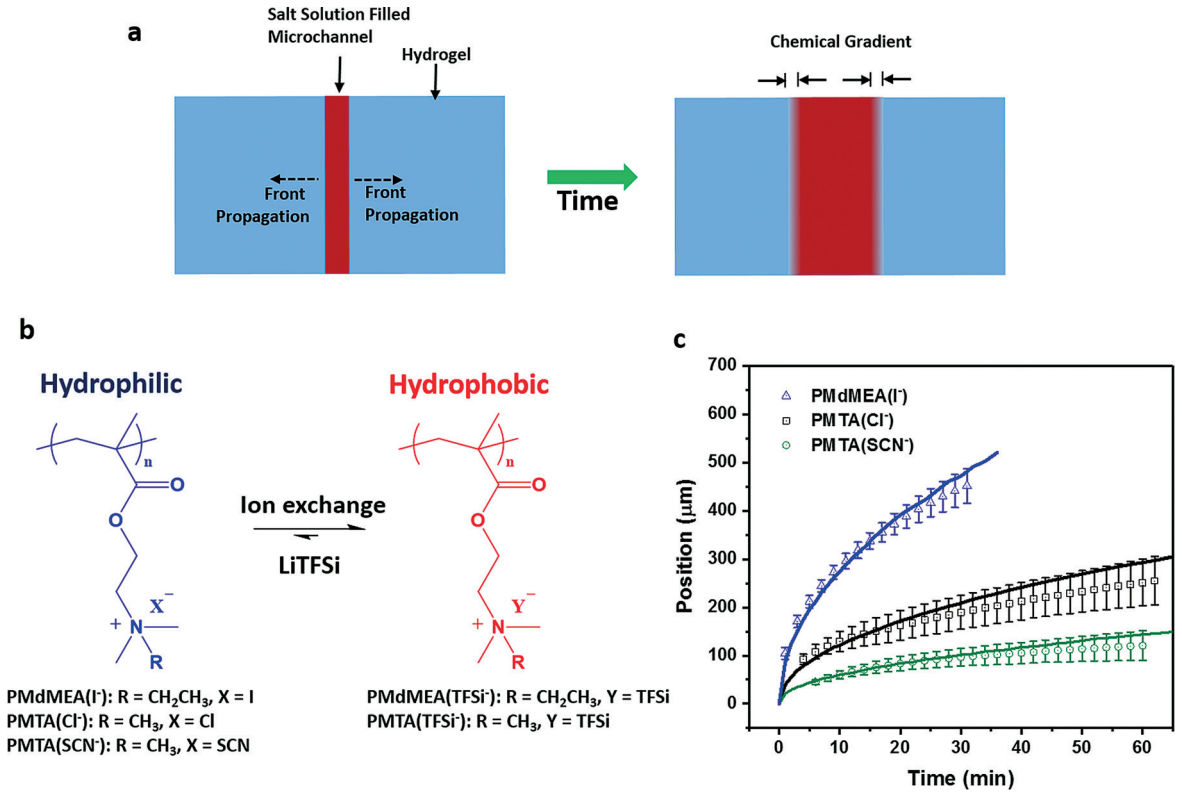

Figure 1. a) Top-view schematic of the dynamic gradient progression. The gradient propagates away from both sides of the microchannel while maintaining a sharp gradient (red, hydrophobic; blue, hydrophilic). b) Investigated hydrogel chemistries. c) Simulated (solid line) and experimentally observed (markers) position of the gradient front as a function of time.

continued propagation of the leading edge of the dynamic gradient. The propagating front can be readily observed under optical microscopy because the water content, and thus refractive index of the hydrogel film changed upon anion exchange (before the ion exchange, the hydrogel is 96 wt.% water, and after the ion exchange it is 31 wt.% water, see Table S2). The gradient positions and the rate of the gradient motion as a function of time and hydrogel chemistry are shown in Figure 1 b,c. Experimentally, it was found the LiTFSi triggered gradients in the poly(*N*-ethyl-2-(methacryloyloxy)-*N*,*N*-dimethylethanaminium iodide) (PMdMEA(I^-)) hydrogels propagated the furthest and fastest among the hydrogels investigated. Using this chemistry, the gradient propagated up to 450 μm in 30 min. Using a poly ([2-(methacryloyloxy)ethyl] trimethylammonium chloride) (PMTA(Cl^-)) hydrogel, the rate of gradient motion was slower, which we ascribe to the fact that PMdMEA(I^-) has an ethyl group vs. the methyl group on PMTA(Cl^-), which enhances the hydrophobic character of the PMdMEA(I^-). $TFSi^-$, a hydrophobic anion, probably shows higher affinity to PMdMEA($TFSi^-$) than to PMTA($TFSi^-$), and the rate of diffusion of $TFSi^-$ through the hydrophobic region to the gradient front, a process that is necessary to keep the gradient moving forward, is probably faster in the more hydrophobic PMdMEA($TFSi^-$). Attempts to utilize hydrogels with quaternary ammonium groups with more and higher order alkyl groups resulted in the formation of precipitates and failure of formation of the propagating front which we attributed to poor solubility of LiTFSi in the ion exchanged region. We also compared PMTA(SCN^-) to PMTA(Cl^-). The Cl^- form is more hydrophilic than the SCN^- form, which increases the kinetics of the ion exchange with $TFSi^-$. Using COMSOL, the gradient position and rate of propagating front were simulated (solid lines) and are found to be in good agreement with the experimental results. COMSOL modeling details can be found in the Supporting Information.

The ion exchange dynamics in the quaternary ammonium hydrogel films can be measured using time-resolved confocal Raman spectroscopy (see Figure S2). As shown in Figure 2 a, the data acquisition point (laser focus) is displaced 300 μm from the microchannel for PMdMEA(I^-), 150 μm for PMTA-(Cl^-), and 100 μm for PMTA(SCN^-). For the system PMTA-(SCN^-), the degree of ion-exchange (DOE) can be measured from the change in Raman peak intensity of the C–F stretching mode for $TFSi^-$ or C–N vibration mode for SCN^- during the ion-exchange (see the SI for details). Importantly, the change in TFSi and SCN is inversely proportional (Figure 2 b). Based on this, we also assume the concentration of Cl^- and I^- is also inversely proportional to the TFSi concentration, enabling the DOE to be calculated for other systems from the C–F peak intensity at 742 cm^{-1} (Figure 2 c). The distance from the start to the end of the gradient length is found from Raman measurement to be short (ca. 20 μm).

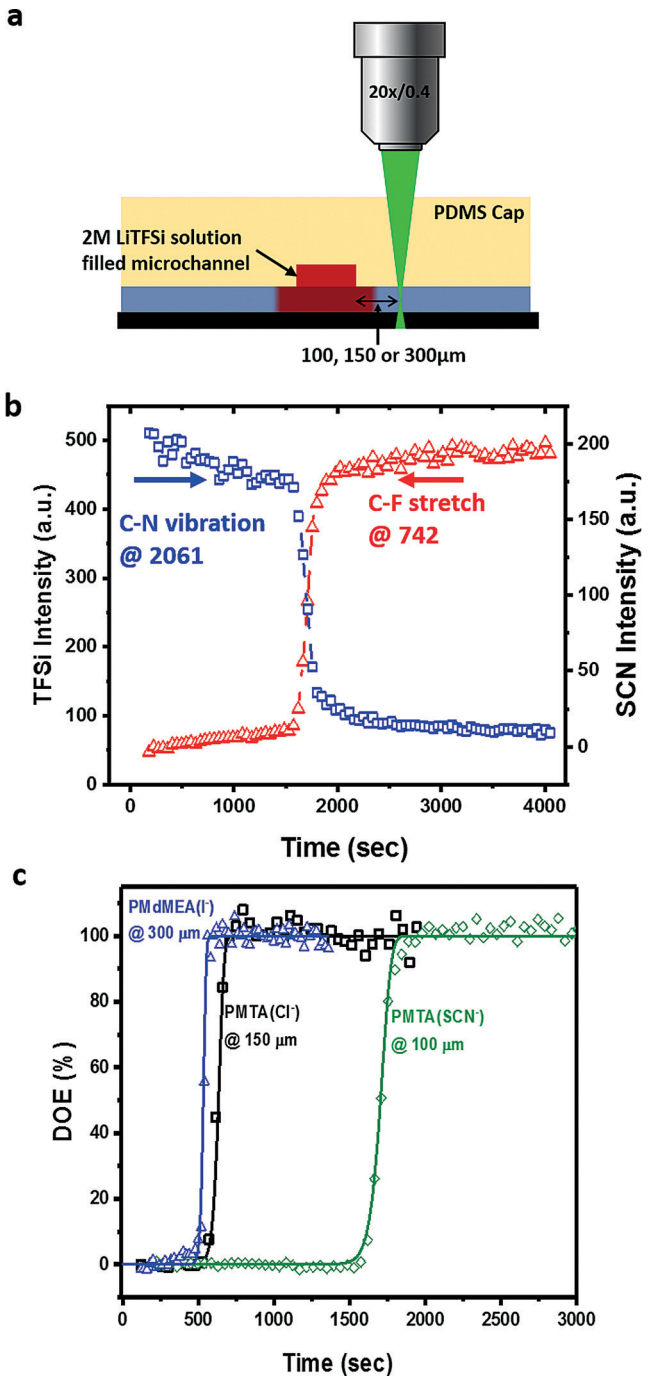

Figure 2. a) Side view schematic of confocal Raman characterization showing the position of the data acquisition point relative to the micro-channel. b) Raman peak intensity at 742 and 2061 cm^{-1} for C–F stretching and C–N vibration for the system PMTA(Cl^-). c) Degree of ion exchange of hydrogel films as a function of time. Solid lines are fitted and markers are experimentally observed.

To understand the dynamics of the traveling wave, and the reason for the sharpness of the gradient, a reaction diffusion equation [Eq. (1) and Eq. (2)] was used.

$$\frac{d[A]}{dt} = D\frac{d^2[A]}{dx^2} - k[A][B] \quad (1)$$

$$\frac{d[B]}{dt} = -k[A][B] \quad (2)$$

$$\mathrm{DOE} = \frac{[B]_{t=0} - [B]_{t=t}}{[B]_{t=0}} \quad (3)$$

where $[A]$ is LiTFSi concentration and $[B]$ is the unexchanged quaternary ammonium concentration. Utilizing the reaction diffusion equations, the diffusion coefficient, D of LiTFSi in the ion exchanged hydrogels and the reaction rate constant, k of the ion exchange process were evaluated using MATLAB (Table 1). Details of the numerical calculations are in the Supporting Information. Values for the diffusion coefficient obtained from PMTA(Cl^-) and PMTA(SCN^-) hydrogel films are similar because both represent the diffusion of LiTFSi in the PMTA($TFSi^-$) films. D calculated from PMdMEA(I^-) hydrogel films is slightly larger than from PMTA(Cl^-) and PMTA(SCN^-) hydrogel films which we suggest is due to the more hydrophobic character of PMdMEA($TFSi^-$) relative to PMTA($TFSi^-$). k values obtained from the PMdMEA(I^-) hydrogel films are about 6- to 10-fold higher than from PMTA(Cl^-) and PMTA(SCN^-) hydrogel films, suggesting that PMdMEA has higher association affinity to TFSi relative to the other two hydrogel films. The k obtained from PMTA(Cl^-) is slightly higher than from PMTA(SCN^-) which agrees well with the association affinity hypothesis as well.

Table 1: Diffusion coefficient (D) and reaction rate constant (k) as determined by fitting the data in Figure 2c.

	D [$\times 10^{-10}$ $m^2 s^{-1}$]	k [$M^{-1} s^{-1}$]
PMTA(Cl^-)	0.54 ± 0.12	1.00 ± 0.06
PMTA(SCN^-)	0.11 ± 0.04	0.65 ± 0.30
PMdMEA(I^-)	2.59 ± 0.09	6.30 ± 0.50

Dynamic gradients were then used to transport 1,3,6,8-pyrenetetrasulfonic acid tetrasodium salt (PTSANa), a hydrophilic anionic fluorescent probe, enabling direct visualization of the dynamic gradient directed transport. PTSANa dyes were first introduced into the hydrogel films (see the SI for details), followed by placement of a PDMS block containing a microchannel, which was then filled with LiTFSi solution to trigger the dynamic gradient (Figure 3a). Fluorescence and bright field images were taken different times (Figure 3b). Initially (time zero), the PTSANa dyes could be found everywhere. Immediately after introduction of LiTFSi solution into the micro-channel, a propagating gradient front appears due to the conversion of the hydrogel film from hydrophilic to hydrophobic. From the fluorescence images, it can be seen that the PTSANa dyes were driven by and concentrated in front of the dynamic gradient. In-situ Raman spectroscopy was used to quantify the dye concentration and confirm that negligible dye was present behind the gradient. As shown in Figure 3a, the data acquisition point is displaced 300 μm for PMdMEA(I^-), 150 μm for PMTA(Cl^-) and 100 μm for PMTA(SCN^-) from the microchannel (different acquisition points are used because the kinetics of the processes are much faster for PMdMEA(I^-) than PMTA(Cl^-)

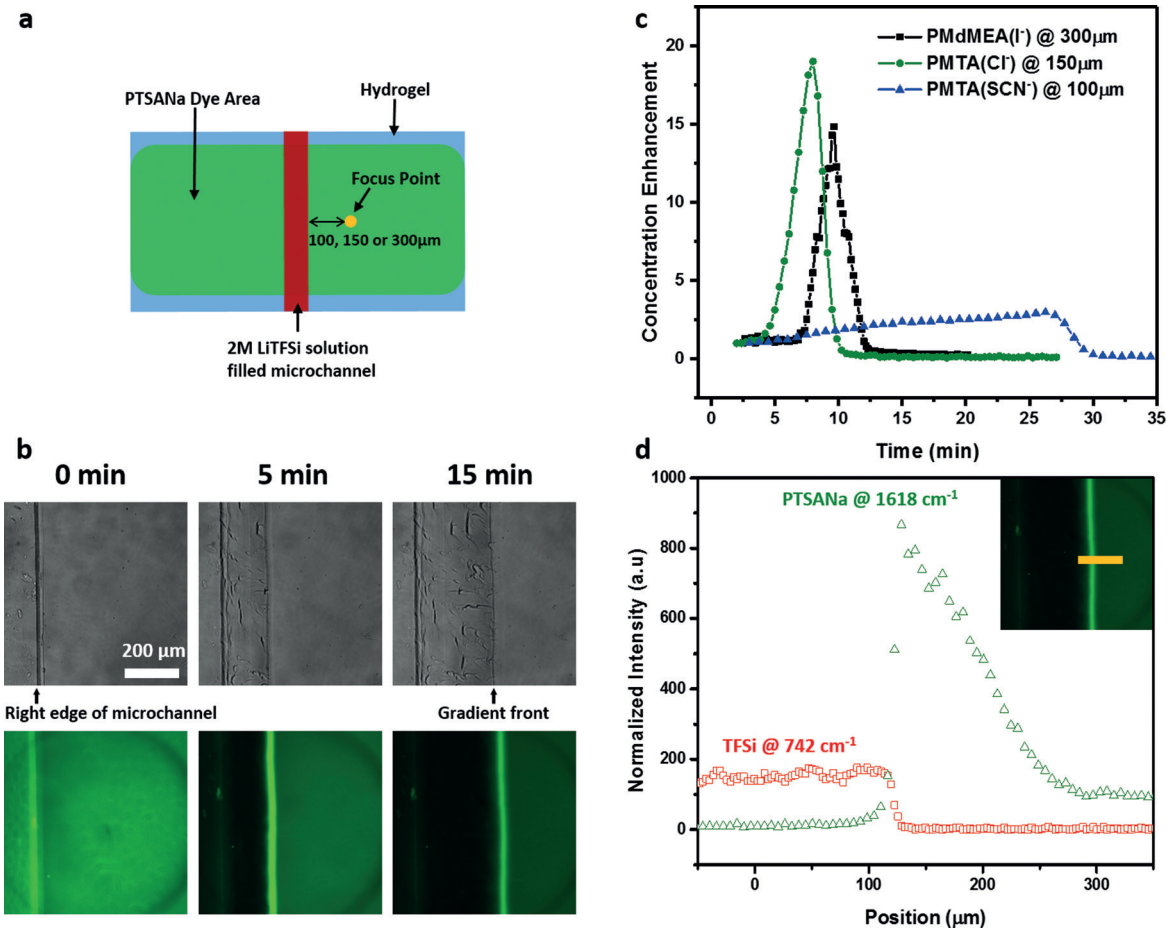

Figure 3. a) Top-view illustration of a PTSANa dye-infilled hydrogel film showing the position of the Raman data acquisition point relative to the microchannel (100, 150 or 300 μm to the right of the microchannel depending on the hydrogel chemistry). b) Fluorescence and bright field images of a PMdMEA(I^-) hydrogel film taken at various times during the directed transport of PTSANa. The right edge of the LiTFSi filled microchannel is indicated at the left. The dynamic gradient propagated from left to right. c) Concentration enhancement as a function of time as determined by the normalized Raman signal intensities of PTSANa. d) Normalized Raman peak intensities of $TFSi^-$ and PTSANa across the propagating front. The Raman spectra was normalized by the C–H stretch of PMdMEA(I^-) at 1448 cm^{-1}. Each point was acquired in 10 s, so the front was effectively stationary during the measurement (the important part of the gradient was measured in around 60 s, a time over which the gradient moved around 10 μm).

and PMTA(SCN^-)). The aromatic structure of PTSANa provides distinct Raman signals (C–C aromatic vibrations at 1201 and 1618 cm^{-1}) enabling the concentration enhancements as a function of time to be calculated by normalizing the intensity of C–C aromatic vibration signals of PTSANa by the original intensity (Figure 3c). The PTSANa concentration starts to increase gradually as the dynamic gradient approaches and reaches a maximum (19-fold in 6 min for PMTA(Cl^-), 150 μm away from the micro-channel) right as the dynamic gradient passes. After the dynamic gradient passes, the signal from PTSANa disappears, indicating that a negligible concentration of dye molecules remain behind the gradient. Using Raman spectroscopy to scan across the propagating front provides additional evidence for the directed molecular transport. As shown in Figure 3d, no PTSANa was detected in the ion-exchanged (hydrophobic) region of hydrogel film, and the PTSANa concentration was significantly enhanced directly in front of the dynamic gradient.

A radial focusing gradient designed to concentrate the PTSANa dye was initiated using an omega-shaped LiTFSi solution-filled micro-channel (Figure 4a). Fluorescence and bright field images were then taken at different times (Figure 4b). Before triggering, the PTSANa dye was uniformly distributed across the hydrogel. After triggering, the dynamic gradient propagated towards the center of the omega, concentrating the PTSANa to a small region (Figure 4b). The interior diameter of the omega-shaped microchannels used for PMTA(Cl^-) and PMdMEA(I^-) hydrogels were 500 μm and 900 μm, respectively (see Figure S5). Using in situ Raman spectroscopy, the gradient directed concentration was quantified, with the data acquisition point near the center of the omega (Figure 4c). The dye concentration rises gradually, and then rapidly as the propagation front approaches the center. Using PMTA(Cl^-) as the hydrogel host, the dye is concentrated 70-fold in about 26 min, and using PMdMEA(I^-) as the hydrogel host, the dye is concentrated 30-fold in about 16 min. The variance in concentration

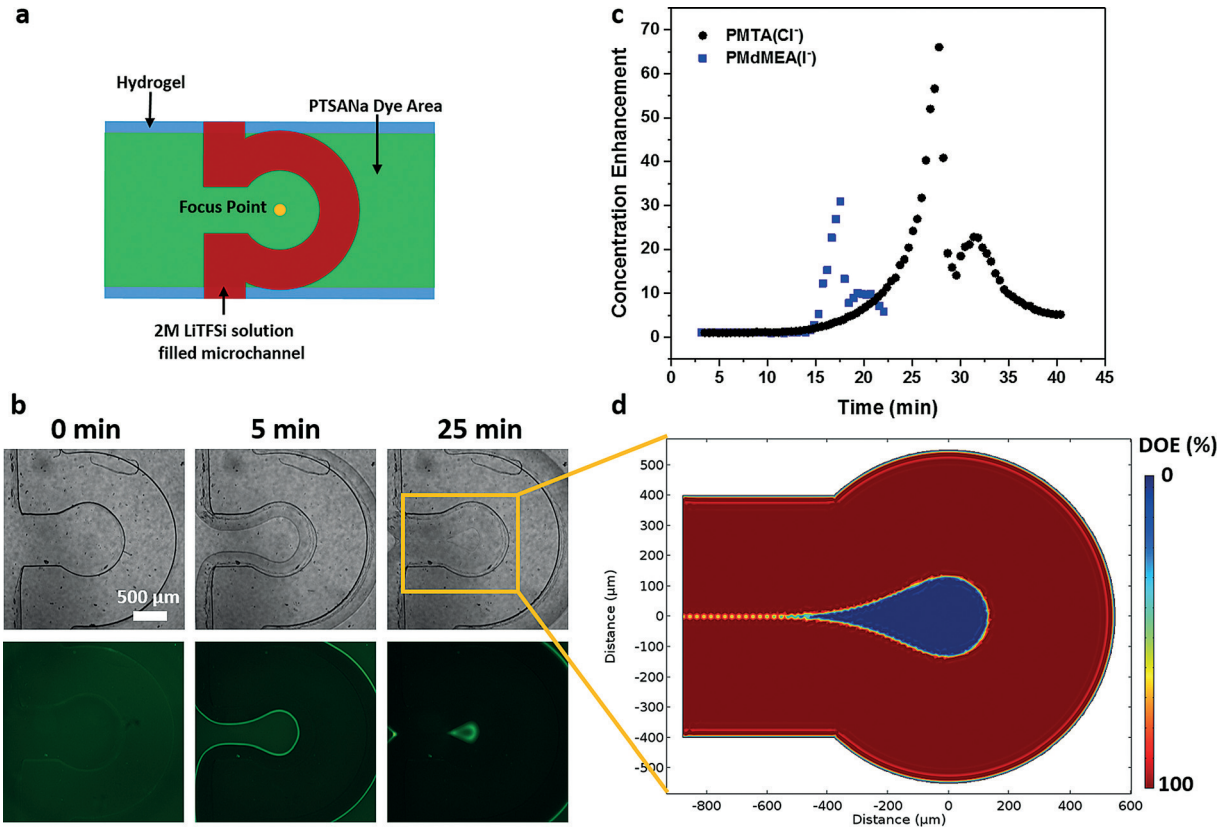

Figure 4. a) Illustration of omega-shaped focusing microfluidic channel (red) and data acquisition point (yellow) on the dye-containing hydrogel film. b) Fluorescence and bright field optical images of a PMdMEA(I^-) hydrogel film taken during the directed concentration of PTSANa. c) Concentration enhancement as a function of time as determined from the Raman intensities of the PTSANa. d) COMSOL simulation of DOE triggered by an omega-shaped microchannel after 25 min. The legend represents the DOE of the hydrogel film.

enhancement between two hydrogel systems can be attributed to the solubility of PTSNa is lower in PMdEA(I^-), and thus simply cannot build up to the same concentration before precipitating and getting trapped behind the moving gradient in the hydrogel. For both hydrogel systems, as the dynamic gradients converged, after peaking, the PTSANa concentration at the focusing point dropped rapidly since the data acquisition point was not exactly at the convergence point. Subsequently, the dye concentration increased slightly and then decreased slowly as the dye which was focused slightly away from the data acquisition point counter-diffused back past the Raman data acquisition point (once the gradient disappears, the driving force for concentration also disappears). We think it is interesting to consider the potential of the concept of a focusing dynamic gradient to advance the detection efficiency and sensitivity of sensors in general, and nanoscale sensors which are limited by the small size of the sensor and free diffusion of analyte in particular.[12]

In summary, we demonstrate that a coupled RD process drives fast gradient motion and enables the gradient to remain sharp as it propagates. It is the slope of the chemical potential within the gradient that provides the driving force for directional transport, and thus sets the upper bound of the molecular transport rate. In qualitative terms, as long as the target molecule has a stronger affinity for the host matrix in front of the gradient relative to behind the gradient, and can diffuse forward under the influence of the gradient faster than the gradient propagates, it will be transported by the traveling wave. As an example of the potential of molecular concentration using this approach, a 70-fold concentration enhancement of a hydrophilic anionic dye was demonstrated. This concentration enhancement is almost certainly not an upper bound.

Acknowledgements

This work was supported by Defense Threat Reduction Agency under award number HDTRA 1-12-1-0035. We thank Dr. Brian Pate (DTRA), and from our laboratory, Dr. Pengcheng Sun for EDS measurements, and Dr. Chunjie Zhang and Dr. Hyung-Jun Koo for helpful discussions.

Conflict of interest

The authors declare no conflict of interest.

Keywords: chemical sensors · dynamic gradient · molecular transport · reaction–diffusion · signal amplification · traveling waves

How to cite: *Angew. Chem. Int. Ed.* **2017**, *56*, 5001 – 5006
Angew. Chem. **2017**, *129*, 5083 – 5088

[1] a) D. Velegol, A. Garg, R. Guha, A. Kar, M. Kumar, *Soft Matter* **2016**, *12*, 4686 – 4703; b) H. Hess, *Annu. Rev. Biomed. Eng.* **2011**, *13*, 429 – 450.
[2] a) T. M. Keenan, A. Folch, *Lab Chip* **2008**, *8*, 34 – 57; b) D. Ishii, M. Shimomura, *Chem. Mater.* **2013**, *25*, 509 – 513; c) R. Walder, A. Honciuc, D. K. Schwartz, *Langmuir* **2010**, *26*, 1501 – 1503; d) A. Perl, A. Gomez-Casado, D. Thompson, H. H. Dam, P. Jonkheijm, D. N. Reinhoudt, J. Huskens, *Nat. Chem.* **2011**, *3*, 317 – 322; e) P. Burgos, Z. Zhang, R. Golestanian, G. J. Leggett, M. Geoghegan, *ACS Nano* **2009**, *3*, 3235 – 3243; f) T. Chang, D. I. Rozkiewicz, B. J. Ravoo, E. W. Meijer, D. N. Reinhoudt, *Nano Lett.* **2007**, *7*, 978 – 980; g) C. Zhang, A. Sitt, H.-J. Koo, K. V. Waynant, H. Hess, B. D. Pate, P. V. Braun, *J. Am. Chem. Soc.* **2015**, *137*, 5066 – 5073; h) A. Sitt, H. Hess, *Nano Lett.* **2015**, *15*, 3341 – 3350.
[3] a) B. A. Grzybowski, *Chemistry in Motion: Reaction-Diffusion Systems for Micro- and Nanotechnology*, Wiley, Hoboken, **2009**; b) E. A. Newman, K. R. Zahs, *Science* **1997**, *275*, 844 – 847; c) B. A. Grzybowski, K. J. M. Bishop, C. J. Campbell, M. Fialkowski, S. K. Smoukov, *Soft Matter* **2005**, *1*, 114 – 128; d) P. Müller, K. W. Rogers, B. M. Jordan, J. S. Lee, D. Robson, S. Ramanathan, A. F. Schier, *Science* **2012**, *336*, 721 – 724.
[4] a) I. R. Epstein, B. Xu, *Nat. Nanotechnol.* **2016**, *11*, 312 – 319; b) S. Kondo, T. Miura, *Science* **2010**, *329*, 1616 – 1620.
[5] I. R. Epstein, V. K. Vanag, A. C. Balazs, O. Kuksenok, P. Dayal, A. Bhattacharya, *Acc. Chem. Res.* **2012**, *45*, 2160 – 2168.
[6] a) T. Arimura, M. Mukai, *Chem. Commun.* **2014**, *50*, 5861 – 5863; b) I. R. Epstein, J. A. Pojman, *An Introduction to Nonlinear Chemical Dynamics*, Oxford University Press, Oxford, **1998**.
[7] a) A. M. Turing, *Philos. Trans. R. Soc. London Ser. B* **1952**, *237*, 37 – 72; b) T. Bánsági, V. K. Vanag, I. R. Epstein, *Science* **2011**, *331*, 1309 – 1312.
[8] R. Yoshida, *Adv. Mater.* **2010**, *22*, 3463 – 3483.
[9] Y. Murase, S. Maeda, S. Hashimoto, R. Yoshida, *Langmuir* **2009**, *25*, 483 – 489.
[10] O. Azzaroni, A. A. Brown, W. T. S. Huck, *Adv. Mater.* **2007**, *19*, 151 – 154.
[11] a) M. C. Gurau, S.-M. Lim, E. T. Castellana, F. Albertorio, S. Kataoka, P. S. Cremer, *J. Am. Chem. Soc.* **2004**, *126*, 10522 – 10523; b) Y. Zhang, P. S. Cremer, *Curr. Opin. Chem. Biol.* **2006**, *10*, 658 – 663; c) D. F. Parsons, M. Bostrom, P. L. Nostro, B. W. Ninham, *Phys. Chem. Chem. Phys.* **2011**, *13*, 12352 – 12367.
[12] J. Fang, S.-C. Park, L. Schlag, T. Stauden, J. Pezoldt, H. O. Jacobs, *Adv. Funct. Mater.* **2014**, *24*, 3706 – 3714.

Manuscript received: January 6, 2017
Revised: February 14, 2017
Final Article published: April 3, 2017

